ACS Catalysis

Research Article

pubs.acs.org/acscatalysis

Nature of WO_x Sites on SiO_2 and Their Molecular Structure–Reactivity/Selectivity Relationships for Propylene Metathesis

Soe Lwin,[†] Yuanyuan Li,[‡] Anatoly I. Frenkel,[‡] and Israel E. Wachs*[,†]

[†]Operando Molecular Spectroscopy and Catalysis Laboratory, Department of Chemical Engineering, Lehigh University, Bethlehem, Pennsylvania 18015, United States

[‡]Department of Physics, Yeshiva University, New York, New York 10016, United States

Supporting Information

ABSTRACT: Supported WO_x/SiO_2 catalysts were investigated for propylene metathesis as a function of tungsten oxide loading and temperature. The catalysts were synthesized by incipient-wetness impregnation of an aqueous ammonium metatungstate solution onto the silica support and calcined at elevated temperatures to form the supported tungsten oxide phase. *In situ* Raman spectroscopy under dehydrated conditions revealed that below 8% WO_x/SiO_2, only surface WO_x sites are present on the silica support: dioxo $(O{=}{=})_2WO_2$ and mono-oxo $O{=}{=}WO_4$. The *in situ* XANES analysis showed that dioxo surface WO_4 sites were the dominant surface WO_x sites on SiO_2 (>90%). The isolated nature of the surface WO_x sites was confirmed with *in situ* UV–vis spectroscopy. The surface WO_x sites are activated by exposure to propylene at elevated temperature that removes oxygen from these sites. The activation process produces a highly active surface WO_x site that can perform olefin metathesis at ~150–250 °C. For 8% WO_x/SiO_2 and higher tungsten oxide loading, crystalline WO_3 nanoparticles (NPs) are also present, and their amount increases with greater tungsten oxide loading. WO_3 NPs, however, are not active for propylene metathesis. The acid character of the surface WO_x sites (Lewis) and WO_3 NPs (Brønsted) is responsible for formation of undesirable reaction products (C_4–C_6 alkanes and dimerization of $C_2^{=}$ to $C_4^{=}$). This study represents the *first time* that molecular level structure–activity/selectivity relationships have been established for propylene metathesis by conventionally impregnated supported WO_x/SiO_2 catalysts.

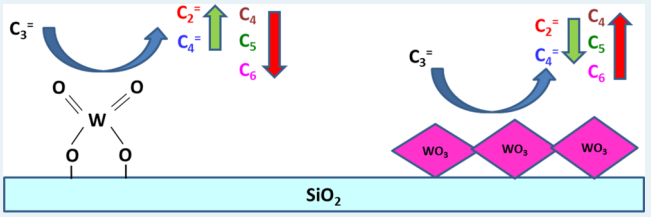

KEYWORDS: *catalyst, supported, tungsten oxide, silica, metathesis, propylene, spectroscopy, in situ, operando, Raman, UV–vis, XAS, TPSR*

1. INTRODUCTION

The olefin metathesis reaction was discovered in the early 1960s and became a commercial process in the late 1960s for the production of ethylene and butene from propylene (Phillips Triolefin Process).[1] Nowadays, the reverse process is economically desired due to a world shortage of propylene caused by the shift to lighter feedstocks derived from shale gas fracking.[1] Although homogeneous metathesis catalysts have received much attention, with well-defined model catalysts that exhibit high activity and selectivity, their commercial applications remain quite limited because of issues related to catalyst recovery and product separation.[2] To circumvent these technical issues, the commercial catalyst employed for the Phillips Triolefin Process employs a heterogeneous supported WO_x/SiO_2 catalyst that operates at 400–600 °C. The supported WO_x/SiO_2 catalyst consists of a tungsten oxide phase deposited on a high surface area SiO_2 support. The advantages of the supported WO_x/SiO_2 catalyst are (*i*) resiliency to trace quantities of oxygenate in the feed that are poisons for metathesis,[2,3] (*ii*) long catalyst lifetime compared to other supported metathesis catalysts based on MoO_x or ReO_x,[2] (*iii*) ease of catalyst regeneration to remove deposited coke,[3] and (*iv*) absence of catalyst embrittlement upon periodic regeneration.[3] The higher operating temperature of the supported WO_x/SiO_2 catalysts, however, also results in some olefin isomerization and cracking that adversely impact the metathesis selectivity.[4,5]

From early Raman spectroscopy, under ambient conditions where the catalyst is hydrated, and H_2-temperature-programmed reduction studies of supported WO_x/SiO_2 catalysts, it was proposed that the catalytic active site is a surface compound and not crystalline WO_3 nanoparticles (NPs), but the molecular structure of the surface WO_x compound was not determined.[6] Van Roosmalen et al. initially proposed that the active surface WO_x sites consist of penta-coordinated mono-oxo $O{=}W(OH)_2(-O-Si)_2$ and $O{=}W(OH)(-O-Si)_3$ coordinated species, but direct evidence for these molecular structures was not provided.[7] Verpoort et al. investigated a support consisting of a thin SiO_2 film on a Si(100) single crystal and reacted the silica layer with $C_5H_5W(CO)_3Cl$ in a PhCl solvent to prepare the model catalyst to examine the nature of the deposited WO_x layer after evaporation of the solvent at 120

Received: February 5, 2016
Revised: March 31, 2016

 © XXXX American Chemical Society

DOI: 10.1021/acscatal.6b00389
ACS Catal. 2016, 6, 3061–3071

°C with angle resolved-XPS in a vacuum.[8−10] The study revealed that the deposited tungsten oxide phase was present as a highly dispersed oxide layer after calcination, and it was proposed that the surface tungsten oxide was present as isolated surface WO_4 and polymeric WO_5 sites contained two Si−O−W bonds and terminated with either W−OH or W═O functionalities. These model XPS studies, however, can only provide the *average* stoichiometry of the surface tungsten oxide sites and not direct molecular structural information. Basrur et al. proposed, without supporting experimental evidence, that dioxo $(O═)_2W(−O−Si)_2$ are the catalytic active sites that become nonstoichiometric upon activation for metathesis.[11] Martin et al. performed EXAFS measurements under ambient conditions on supported WO_x/SiO_2 catalysts under ambient conditions and concluded that either hydrated polytungstate chains or Si-containing Keggin-type clusters are present on silica.[12] Several more recent publications about olefin metathesis by supported WO_x/SiO_2 catalysts have been reported, but the characterization studies were also performed under ambient conditions[13−19] where only hydrated polyoxo $(W_{12}O_{39})^{6−}$ clusters and WO_3 NPs are known to be present.[20,21] These studies, however, incorrectly assigned the Raman bands of the hydrated polyoxo tungsten oxide clusters as those belonging to dehydrated surface WO_x sites because of an earlier incorrect assignment by in the literature by Huang et al.[19] The molecular and electronic structures of the tungsten oxide phases on silica have been determined by Wachs et al. combining *in situ* Raman and UV−vis spectroscopy.[20−23] Under ambient conditions, hydrated polyoxo $(W_{12}O_{39})^{6−}$ clusters are the dominant surface tungsten oxide species,[20,23] and WO_3 nanoparticles (NPs) are also present with increasing tungsten oxide loading. Under dehydrated conditions, the hydrated tungsten oxide polyoxo clusters decompose to isolated surface dioxo, $(O═)_2W(−O)_2$, and mono-oxo $O═W(−O)_4$ species, and the WO_3 NPs remain unchanged.[20−23]

In well-defined silica-supported organometallic systems, organic precursors are grafted onto partially dehydroxylated silica (at 200−800 °C), and these systems are able to perform metathesis of both linear and functionalized olefins at relatively low temperatures (<100 °C).[24−29] Some of the W-organic precursors reported in the recent literature are $[(≡Si−O−)W(═O)Me_3]$,[24] $[W(═O)(═CHtBu)−(SHMT)_2-(PMe_2Ph)]$,[25] $[W(═O)(═CHtBu)(SHMT)_2]$ (SHMT = 2,6-dimesitylthiophenoxide),[25] $(ArO)_2W(═O)(═CHtBu)$ (ArO = 2,6-mesitylphenoxide),[26] $[WOCl_4]$ with $SnMe_4$,[27] $WONp_4$, Np = CH_2−tBu,[28] and $[WO(CH_2SiMe_3)_3Cl]$.[29] These well-defined systems have been characterized with NMR, XANES/EXAFS, and IR experiments and DFT calculations. Although their catalytic activity is extremely high, such catalysts cannot be applied in practice to large scale olefin metathesis systems due to their air sensitive nature and inability to regenerate such catalysts. These model silica-supported organometallic catalysts, however, are providing many fundamental insights about the olefin metathesis reaction.

In the present investigation, systematic *in situ* and *operando* UV−vis, XAS (XANES/EXAFS), and Raman spectroscopy under dehydrated and metathesis reaction conditions with transient and steady-state reaction measurements were utilized. This is the first study to report on the nature of the supported tungsten oxide phase on silica during the olefin metathesis reaction that allows establishing the molecular structure−activity/selectivity relationships for propylene metathesis by conventionally impregnated supported WO_x/SiO_2 catalysts.

2. EXPERIMENTAL SECTION

2.1. Catalyst Synthesis. The SiO_2 support (Cabot, BET surface area = 332 m^2/g) was water treated and dried under ambient conditions overnight before being calcined in air at 500 °C for 4 h. Incipient-wetness impregnation of WO_x is achieved by using ammonium metatungstate hydrate, $((NH_4)_6H_2W_{12}O_{40}\cdot xH_2O$, Pfaltz and Bauer, 99.5%) in an aqueous solution of water. The samples were initially dried at RT overnight, then at 120 °C in the air for 2 h before being calcined in the air at 500 °C for 4 h.

2.2. *In Situ* UV−vis Spectroscopy. The UV−vis spectra of the catalyst samples were taken using a Varian Cary 5E UV−vis−NIR spectrophotometer with the Harrick Praying Mantis accessory. Approximately 5−25 mg of each catalyst in finely ground powder form was loaded into an *in situ* environmental cell (Harrick, HVC-DR2). Spectra of the dehydrated samples were collected in the 200−800 nm range at 25 °C, after the 500 °C dehydration, using a scan rate of 15 nm/min and a signal averaging time of 0.6 s. A magnesium oxide sample was used as a standard for obtaining the background absorbance. The Kubelka−Munk function $F(R_\infty)$ was calculated from the absorbance of the UV−vis spectra. The edge energy (E_g), or band gap, was determined by finding the intercept of the straight line for the low-energy rise of a plot of $[F(R_\infty)h\nu]^2$ versus $h\nu$, where $h\nu$ is the incident photon energy. An example of this calculation can be found elsewhere.[30] For the *in situ* UV−vis experiments, the supported $8\%WO_x/SiO_2$ catalyst was dehydrated at 500 °C in 10% O_2/Ar before the temperature was lowered to 300 °C under the flow of the same gas, and the first spectrum was taken. The gas flow was then switched to Ar and then to 1% $C_3^=$/He. The *in situ* UV−vis spectra were collected at 300, 350, and 400 °C under flowing 1% $C_3^=$/He. The catalyst was allowed to stabilize for 30 min at each reaction temperature before the spectrum was recorded. The flow rate of 30 mL/min is used for all gases in these *in situ* experiments.

2.3. *In Situ* and *Operando* Raman Spectroscopy. The Raman spectra of silica supported tungsten oxide catalysts were obtained with a Horiba-Jobin Ybon LabRam HR instrument equipped with three laser excitations (532, 442, and 325 nm) and a liquid N_2-cooled CCD detector (Horiba-Jobin Yvon CCD-3000 V). The 442 nm laser was chosen since it minimized sample fluorescence. Spectral resolution was approximately 2 cm^{-1}, and the wavenumber calibration was checked using the silica standard line at 520.7 cm^{-1}. The lasers were focused on the samples with a confocal microscope using a 50× objective (Olympus BX-30-LWD). Typically, the spectra were collected for 30 s/scan and five scans with a 200 μm hole. Approximately 5−25 mg of each catalyst in powder form was loaded into an environmental cell (Harrick, HVC-DR2) with a SiO_2 window and O-ring seals, which was kept cool by flowing water. The *in situ* Raman spectra of the dehydrated catalysts were collected at room temperature after 500 °C dehydration in 10% O_2/Ar for 30 min. A flow rate of 30 mL/min of 1% propylene/Ar (balance) was used for the *operando* Raman studies during propylene metathesis at 300 °C. The gaseous effluent was simultaneously recorded with an online mass spectrometer (Varian, 1200L quadrupole).

2.4. *In Situ*/*Operando* XAS (XANES/EXAFS) Spectroscopy. W L_1-edge X-ray absorption spectroscopy (XAS) measurements were performed in transmission mode at the beamlines X19A and X18B at the National Synchrotron Light Source (NSLS) at the Brookhaven National Laboratory, using ionization chamber detectors for measuring incident and transmitted beam intensities. In addition, a third ionization chamber was used to detect the beam through a reference W foil for energy calibration and alignment purposes. A quartz capillary cell (I.D./O.D. = 0.8/1.0 mm) was used for *in situ* dehydrated measurements. Data processing and analysis were performed using Athena and Artemis software. The *in situ* XAS spectra of the dehydrated catalysts were collected at a reaction temperature of 300 °C after 500 °C dehydration in $20\%O_2$/He for 30 min. Reference compounds, $Ce_2(WO_4)_3$ (Strem, 99.9%), $H_3PW_{12}O_{40}\cdot nH_2O$ (Sigma-Aldrich, 99.995%), and WO_3(Alfa Aesar, 99.8%), are diluted with boron nitride to have a metal loading of 2−5% and measured under ambient conditions. Only tungstophosphoric acid, $H_3PW_{12}O_{40}\cdot nH_2O$

DOI: 10.1021/acscatal.6b00389
ACS Catal. 2016, 6, 3061−3071

(also diluted with boron nitride), was measured under both ambient and dehydrated conditions (150 °C in 20% O_2/He for 30 min). This dehydration was performed to remove adsorbed moisture. For the *in situ* XAS experiments, after the aforementioned dehydration procedure, the catalysts were cooled down to 300 °C in He. Then, a flow of 1% $C_3^=$/He was introduced at a rate of 10 mL/min, and the spectra were recorded as a function of time. The gaseous products were simultaneously analyzed online with a residual gas analyzer (RGA, Stanford Research System).

2.5. Temperature-Programmed Surface Reaction (TPSR) Spectroscopy. The temperature-programmed surface reaction experiments were performed using an Altamira Instruments (AMI-200) system. The outlet gases were connected to an online mass spectrometer (Dymaxicon Dycor, DME200MS) and a TCD detector for analysis. Typically, ∼100−300 mg of catalyst was loaded into the U-tube reactor. Blank tests with known concentrations of olefins were run for the mass spectrometer (MS) calibration before the experiments. The signals for the mass spectra were also normalized with catalyst weight for comparison. The following MS m/z values were used for detection of the reactants and products: propylene (m/z = 42), ethylene (m/z = 27), 2-butene (m/z = 56), acetaldehyde (m/z = 43), formaldehyde (m/z = 30), carbon dioxide (m/z = 44), acetone (m/z = 58), O_2 (m/z = 32), and water (m/z = 18). The MS cracking patterns were carefully determined with blank runs using the calibration gases and used to correct for the background MS signals. Cracking of propylene gives rise to m/z = 43, and the propylene cracking contributions to CH_3CHO (m/z = 43) were subtracted from the final MS signals. Cracking of 2- butene gives rise to m/z = 27, 28, 30, and 41 values. Unless otherwise noted, the catalysts were dehydrated in 10% O_2/Ar at 500 °C (30 mL/min) for 30 min and cooled in flowing Ar (30 mL/min) to the reaction temperature. The desired reactant amount is achieved by diluting the 5% $C_3^=$/Ar with additional Ar.

2.6. Steady-State Reaction Studies. The catalytic activity measurements were performed in a fixed-bed catalytic reactor under differential conditions (propylene conversion <15%). A separate molecular sieve moisture trap was installed in the inlet propylene gas line to purify the reactants. Both inlet and outlet gas lines were heated using external electric heaters to ∼200 °C to prevent condensation of the reactants and products. The catalysts were pretreated in 10% O_2/Ar at 500 °C for 30 min before cooling down in Ar to 300 °C. Then, a gas mixture of 1% C_3H_6/Ar was introduced at a rate of ∼100 mL/min. The products were analyzed using an online gas chromatograph (Agilent GC 6890) equipped with flame ionization (Agilent Serial #: USC250823H) and thermal conductivity (Restek Product #: PC3533) detectors. Conversion was normalized with propylene flow rate and catalyst weight to obtain the propylene metathesis reactivity (mmol/g/h). The reactivity is computed from

$$\text{reactivity}\left(\frac{\text{mmol}}{\text{g}\times\text{hr}}\right) = \left[\text{conversion}\times\text{concentration}\times\text{flow rate}\left(\frac{\text{mL}}{\text{min}}\right)\times\left(60\frac{\text{min}}{\text{hr}}\right)\times\left(\frac{1}{1000}\frac{\text{L}}{\text{mL}}\right)\right] \Big/ \left[\left(22.4\frac{\text{L}}{\text{mol}}\right)\times\text{loading weight (g)}\right] \quad (1)$$

The conversion of propylene is computed from the change of its GC area with and without the catalyst at each reaction condition. Selectivity of a product (S_i) is obtained from dividing its GC area (x_i) from the total area of all products, X (excluding the reactant propylene), which can mathematically be expressed as

$$S_i = \frac{x_i}{X}\times 100 \quad (2)$$

3. RESULTS

3.1. *In Situ* UV−vis Spectroscopy. The *in situ* UV−vis E_g values of the dehydrated supported WO_x/SiO_2 catalysts along with those of references are shown in Figure 1. The reference E_g values for tungsten oxide isolated and oligomeric structures

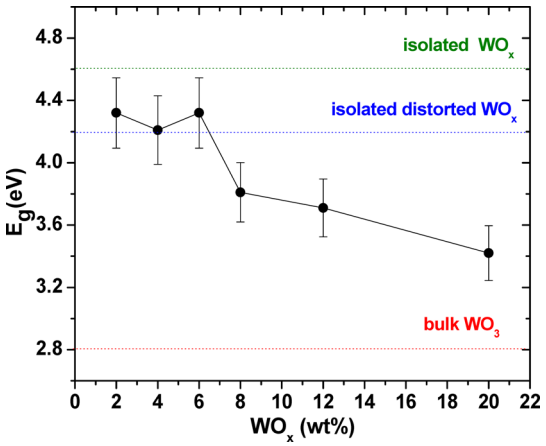

Figure 1. *In situ* UV−vis E_g values for the dehydrated supported WO_x/SiO_2 catalysts as a function of surface tungsten oxide coverage with those of reference compounds.

are taken from ref 20. Distortion of isolated WO_4 sites has a modest effect and decreases the E_g value from 4.6 to 4.2 eV. Below 8% WO_x/SiO_2, the E_g values for the dehydrated catalysts are ∼4.2−4.3 eV, indicating the presence of isolated WO_x sites on the silica support. Above 6% WO_x/SiO_2, the E_g value monotonically decreases from ∼4.2 to 3.4 eV with increasing tungsten oxide loading. The decreasing E_g values reflect the presence of larger WO_x domains and are related to the presence of crystalline WO_3 nanoparticles (NPs) in these catalysts, which will be shown below with the corresponding Raman spectroscopy.

The *in situ* UV−vis spectra during the propylene metathesis reaction are presented in Figure 2a. The curves in flowing O_2/Ar and Ar are identical, and only the latter is evident in Figure 2a since the Ar curve overlaps the O_2/Ar curve. The difference spectra in Figure 2b were obtained by subtracting the fully oxidized spectrum from the spectra during reaction. Introducing Ar after the O_2/Ar pretreatment does not form UV−vis d−d bands of reduced WO_x in the 300−800 nm region, indicating that the WO_x sites on SiO_2 do not undergo detectable reduction in the inert environment. During propylene metathesis, the intensity of the W^{6+} LMCT band at ∼260 nm decreases, and weak d−d band(s) from reduced WO_x sites appear in the ∼300−800 nm region. The UV−vis spectra of reduced WO_x compounds give rise to d−d transitions: W^{5+} in tris(pyrazolyl)borato-oxo-tungsten and $(Et_4N)[WO(S_2C_2Ph_2)_2]$ complexes exhibit bands at 470 and 720 nm,[31,32] and W^{4+} in the WO_2 reference compound exhibits broad bands at 410 and 460 nm (see Figure 2b). The weak and broad UV−vis bands in the difference spectra during reaction suggest that some reduced surface W^{5+} and W^{4+} sites are present during propylene metathesis, but these weak and broad bands are not well-resolved to assign. The absence of strong UV−vis d−d bands for reduced surface WO_x sites probably reflects the oxidation of the reduced surface WO_x sites by the surface intermediates back to W^{6+} (see section below on catalyst activation). The presence of W^{5+} sites have been reported for olefin metathesis over supported WO_x/Al_2O_3 and WO_x/ZrO_2[33,34] catalysts with EPR spectroscopy. EPR spectroscopy, however, cannot detect W^{4+} sites since they are not

DOI: 10.1021/acscatal.6b00389
ACS Catal. 2016, 6, 3061−3071

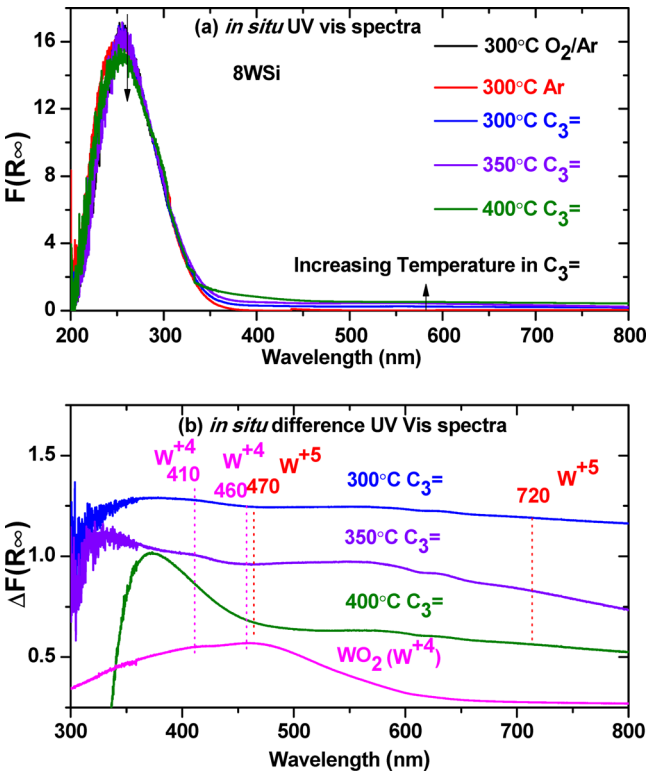

Figure 2. *In situ* UV−vis spectra of the supported 8%WO_x/SiO_2 catalyst (a) during propylene metathesis and (b) difference spectra along with that of the bulk WO_2 reference compound.

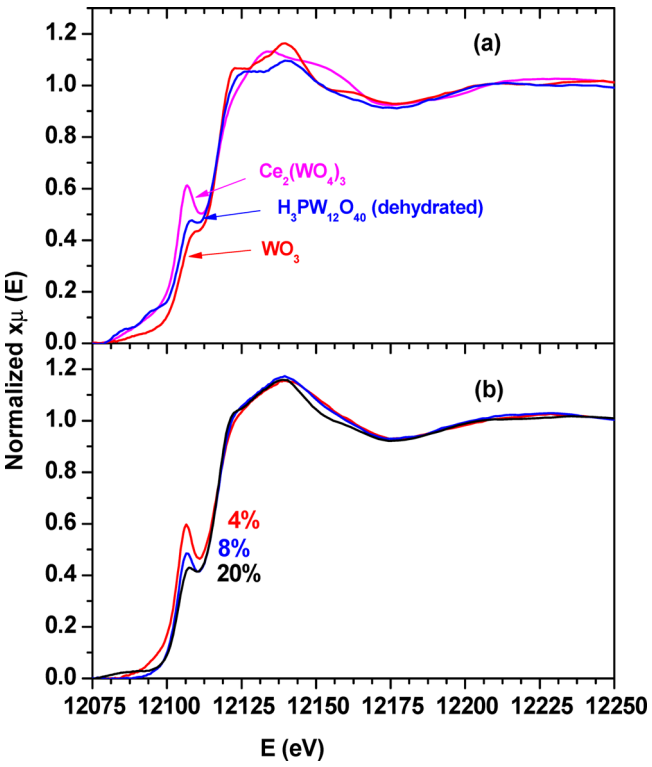

Figure 3. *In situ* W L_1 edge XANES spectra of (a) reference materials and (b) dehydrated supported WO_x/SiO_2 catalysts.

paramagnetic. These EPR measurements did not detect W^{3+}, which is paramagnetic, and reflect the absence of W^{3+} sites during olefin metathesis by supported WO_x catalysts.

3.2. *In Situ* W L_1-XANES and EXAFS Spectroscopy. The *in situ* W-L_1 XANES spectra of several reference materials with known structures and the dehydrated supported WO_x/SiO_2 catalysts are presented in Figure 3. The intensity of the XANES pre-edge peak increases when the absorbing atom (W) is displaced from the inversion symmetry center, resulting in a strong pre-edge feature for WO_4 coordinated structures and a weak pre-edge feature for WO_6 coordinated structures.[35,36] The bulk $Ce_2(WO_4)_3$ reference compound contains only isolated WO_4 sites,[37] and consequently, its XANES spectrum has a strong pre-edge feature. Bulk crystalline WO_3 is composed of WO_6-coordinated units with a more symmetric environment, and thus, its XANES pre-edge feature is quite small. Dehydrated crystalline $H_3PW_{12}O_{40}$ contains highly distorted mono-oxo WO_6 sites that deviate from the more symmetric environment of WO_3 giving rise to a weak XANES pre-edge peak. The dehydrated supported 4% WO_x/SiO_2 catalyst exhibits almost the same pre-edge intensity as bulk $Ce_2(WO_4)_3$. Comparison of the intensity of the XANES pre-edge peaks for the dehydrated supported 4% WO_x/SiO_2 catalyst and $Ce_2(WO_4)_3$ suggests that the catalyst contains ~92% WO_4-coordinated and ~8% WO_6-coordinated sites. The intensity of the XANES pre-edge for the supported 8% and 20% WO_x/SiO_2 catalysts decreases with tungsten oxide loading reflecting the additional presence of a WO_6-coordinated structure, which is crystalline WO_3 nanoparticles (NPs; see Raman section below). Comparison of the XANES pre-edge intensity of the supported 8 and 20% WO_x/SiO_2 catalysts with that of the supported 4% WO_x/SiO_2 catalyst suggests that the catalysts with higher tungsten oxide loading contain ~25 and ~60% WO_3 NPs, respectively.

The corresponding *in situ* W L_1 EXAFS spectra provide information about the radial distribution of W−O bonds. The k^2 -weighted EXAFS spectra of the reference materials and dehydrated supported WO_x/SiO_2 catalysts are shown in Figure 4. All spectra exhibit distinct peaks assigned to W−O contribution in the range of 1−2 Å. As shown in Figure 4a, there are differences in W−O peak intensities and positions, reflecting the differences in W−O coordination environments between different reference compounds. The EXAFS spectra of the dehydrated supported WO_x/SiO_2 catalysts (Figure 4b) exhibit similar spectral features. The intensity of the W−O peak (at ~1.2 Å) is dependent on WO_x loading, suggesting the coordination number and distribution of W−O bond changes as a function of WO_x loading. To obtain quantitative information on the W−O bonding environment, EXAFS analysis of the reference $Ce_2(WO_4)_3$ and the dehydrated supported WO_x/SiO_2 catalysts were performed. First, we analyzed the $Ce_2(WO_4)_3$ compound in order to obtain the amplitude factor (found to be 0.64 ± 0.09), assuming the tetrahedral coordination of W by O atoms. Then, the amplitude factor was fixed to 0.64 and applied to all data sets of catalysts. We performed fitting of all catalysts simultaneously and examined two models: (1) varying the coordination number (N) of W−O bonds while requiring that the disorder factor (σ^2) of the W−O bond is the same for all the data sets and (2) varying both N and σ^2 for all the data. The fitting quality using the two models is comparable, and they have similar reduced chi-squared and R factors. Due to the strong N−σ^2 correlation, the W−O coordination number could not be obtained reliably from EXAFS analysis, but the best fit values of the W−O bond distances provided important insights. In both analysis models,

DOI: 10.1021/acscatal.6b00389
ACS Catal. 2016, 6, 3061−3071

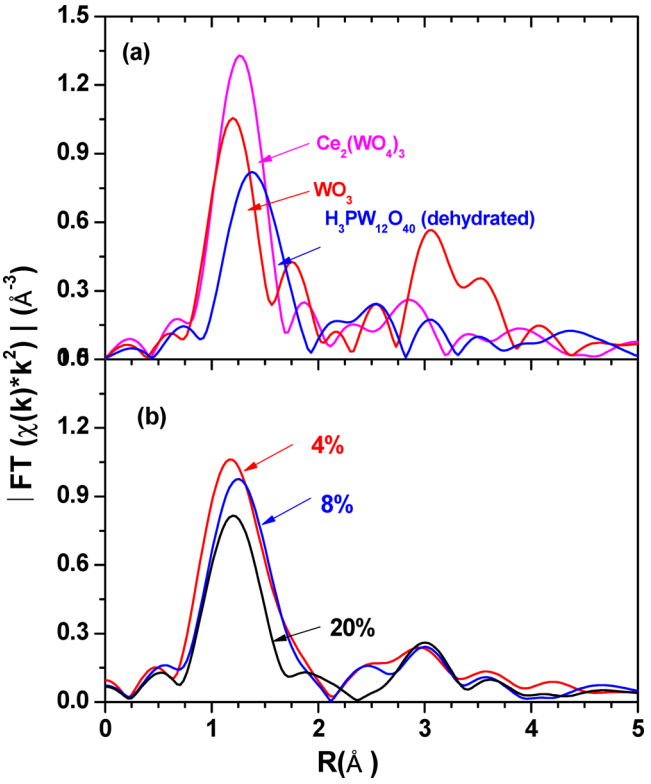

Figure 4. Magnitudes of Fourier-transformed, not-phase-corrected, k^2-weighted W L_1-edge EXAFS spectra in the R space for the (a) reference materials and (b) dehydrated supported WO_x/SiO_2 catalysts. For all the data, the k range for Fourier transformation is 2−9 $Å^{-1}$.

the average W−O bond distances are found to be similar for all WO_x/SiO_2 catalysts (1.83 ± 0.02 Å for 4%, 1.87 ± 0.03 Å for 8%, and 1.82 ± 0.02 Å for 20% WO_x/SiO_2) suggesting that all the catalysts are dominated by a W−O short bond that is known to be present for surface WO_x sites on SiO_2.[22]

The *in situ* XANES spectra of the supported 4% and 20% WO_x/SiO_2 catalysts during propylene metathesis at 300 °C are shown in Figure S1. The supported 4%WO_x/SiO_2 catalyst is free of WO_3 NPs (see UV−vis section above and Raman section below) and exhibits almost no decrease in the intensity of the XANES pre-edge peak during propylene metathesis. The supported 20% WO_x/SiO_2 catalyst that contains a significant amount of crystalline WO_3 NPs (UV−vis section above and Raman section below); however, it also does not exhibit an apparent decrease in the intensity of the XANES pre-edge peak during propylene metathesis. The k^2 weighted W L_1-edge EXAFS data of the supported WO_x/SiO_2 catalysts are presented in Figure S2 and do not undergo any significant changes. The corresponding *operando* MS spectra for both catalysts are shown in Figure S3.

3.3. *In Situ*/*Operando* Raman Spectroscopy. The *in situ* Raman spectra of the dehydrated supported WO_x/SiO_2 catalysts before olefin metathesis are presented in Figure 5. The Raman spectra are normalized with respect to the 495 cm^{-1} band of the SiO_2 support. The silica support gives rise to Raman bands at 410−415, 487, 605, 810, and 970 cm^{-1} that have been assigned to network bending modes, D1 and D2 defect modes related to tri- and tetra-cycloxiloxane rings, Si−O−Si symmetrical stretching, and Si−OH stretching mode of the surface hydroxyls, respectively.[22] The supported 4% and 6% WO_x/SiO_2 catalysts exhibit additional Raman bands at 1016, 985, and 350 cm^{-1} from dioxo ν_s $[(O{=})_2WO_2]$ stretch and mono-oxo ν_s $[O{=}WO_4]$ stretch and their associated bending modes at ∼350 cm^{-1}, respectively.[22] The small shoulder at ∼968 cm^{-1} is the ν_{as} $[(O{=})_2WO_2]$ vibrational stretch of the surface dioxo site. The ratio of the raw Raman bands for the dioxo/mono-oxo surface WO_x sites is ∼1.5 and ∼2.5 for the supported 2 and 4% WO_x/SiO_2 catalysts, respectively, and decreases to ∼0.7 for supported 8 and 20% WO_x/SiO_2 catalysts (see Figure S4a and b in the SI). Switching the gaseous environment from He to O_2/He has a minimal effect on the dioxo/mono-oxo ratio (see Figure S5). The absence of Raman bands from bending W−O−W vibrations in the ∼200−300 cm^{-1} region demonstrates that the surface WO_x sites are isolated, which is in agreement with the UV−vis findings above. Crystalline WO_3 NPs (Raman bands at ∼265, ∼325, ∼715, and ∼806 cm^{-1}) have a Raman cross-section that is significantly stronger than the surface WO_x sites[38] and are not present for the supported 4% and 6% WO_x/SiO_2 catalysts but are clearly present for supported 8% WO_x/SiO_2 and higher tungsten oxide loadings. The Raman bands of the symmetric stretches of the surface dioxo WO_4 and mono-oxo WO_5 sites slightly blue shift in the presence of the crystalline WO_3 NPs. The Raman spectra reveal that tungsten oxide is 100% dispersed on SiO_2 below 8% WO_3/SiO_2 for the current set of synthesized catalysts, which is in agreement with the above UV−vis findings.

The *operando* Raman spectra of the supported 4% and 8% WO_x/SiO_2 catalysts during propylene metathesis are presented in Figures 6 and 7 with the bands normalized by employing the SiO_2 vibrations at 815 cm^{-1} for the 4% catalyst and 495 cm^{-1} for the 8% catalyst as internal standards. The strong 805 cm^{-1} band for WO_3 crystals prevents monitoring of the SiO_2 815 cm^{-1} band as an internal standard for the 8%WO_x/SiO_2 catalyst. Therefore, the silica Raman band at the 495 cm^{-1} band was used as an internal standard for the 8%WO_x/SiO_2 catalyst. Prior to propylene metathesis, the catalyst were always flushed with flowing Ar to remove gas phase molecular O_2 before beginning the flow of $C_3^{=}$/Ar. The Raman spectra in flowing 10% O_2/Ar and Ar were the same in both environments. The *in situ* Raman spectra of the supported 4% WO_x/SiO_2 catalyst (Figure 6a) indicate that the intensity of the Raman bands of both surface dioxo $(O{=})_2WO_2$ and mono-oxo $O{=}WO_4$ sites decrease during propylene metathesis, and both bands are present for at least ∼100 min of reaction. The intensity of the Raman bands from both surface WO_x sites selectively decrease with reaction time relative to the irreducible SiO_2 support. This indicates that both surface WO_x sites have been activated by a loss of W=O oxo bond formation of surface $W{=}CH_2/W{=}CHCH_3$ intermediates and that the intensity decrease is not related to deposition of carbonaceous deposits. The decrease in W=O vibrations is due to removal of oxygen and coordination of olefins and their reaction intermediates to the surface WO_x sites. Within experimental error, it is difficult to determine if one of the surface WO_x sites reduces faster than the other. The corresponding simultaneous MS signals confirm that the propylene metathesis reaction is taking place and that the MS ratio of $C_2^{=}/C_4^{=}$ ∼ 1. Both surface WO_x sites remain dispersed on the silica support during propylene metathesis since reoxidation does not reveal crystalline WO_3 NPs and the relative ratio of the surface dioxo/mono-oxo is the same at the beginning of the reaction and after reaction. The behavior of crystalline WO_3 NPs during propylene metathesis is presented in Figure 7 for the supported 8% WO_x/SiO_2 catalyst. The

DOI: 10.1021/acscatal.6b00389
ACS Catal. 2016, 6, 3061−3071

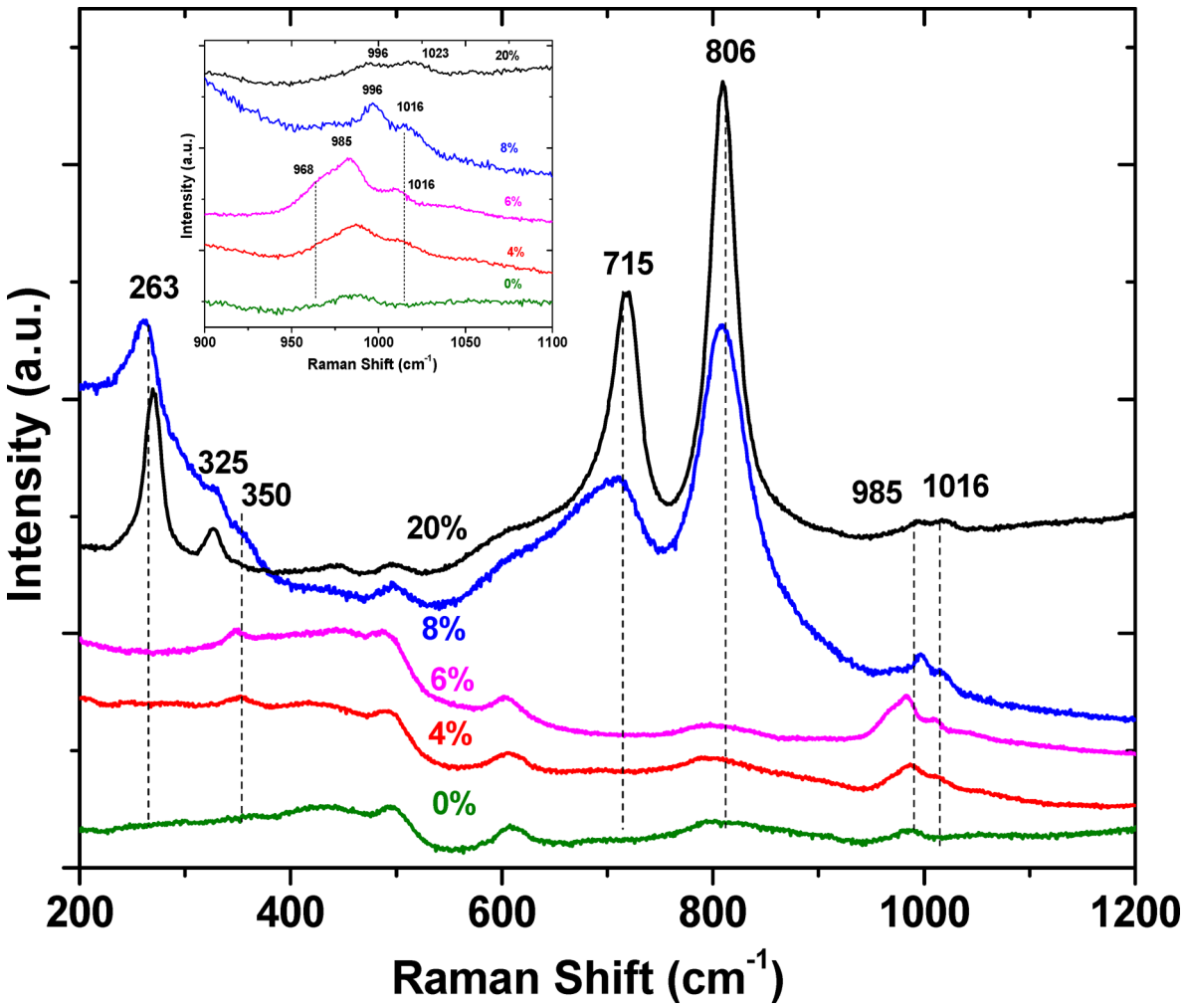

Figure 5. *In situ* Raman spectra (442 nm) of the supported WO_x/SiO_2 catalysts under dehydrated conditions (flowing O_2/Ar at 300 °C). Inset shows the 900−1100 cm^{-1} region.

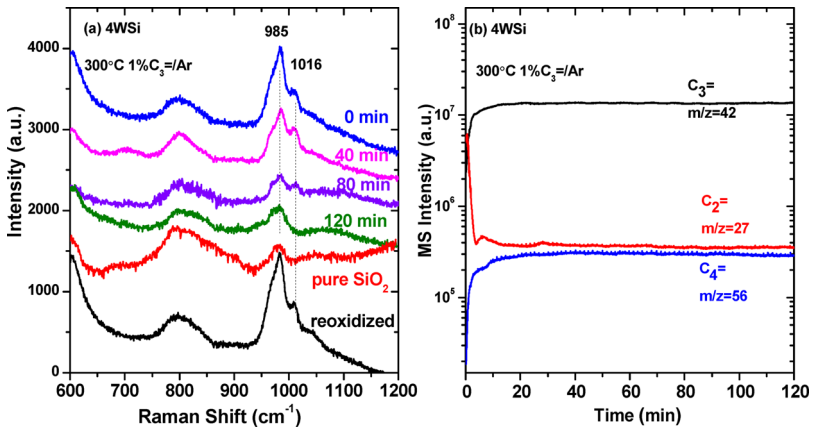

Figure 6. (a) *Operando* Raman spectra (442 nm) of the supported 4%WO_x/SiO_2 catalyst (Raman spectrum of pure SiO_2 is shown for comparison) at 300 °C and (b) its simultaneous MS spectra for main products. The catalyst was reoxidized in 10% O_2/Ar at 500 °C for 30 min after the reaction (Raman spectra normalized against SiO_2 band at 815 cm^{-1}). Propylene conversion was ∼4%.

intensity of the Raman bands for the crystalline WO_3 NPs monotonically decreases with propylene metathesis reaction time, indicating reduction of these sites. Complete recovery of the intensity of the Raman bands from the crystalline WO_3 NPs is obtained upon reoxidation, indicating that the loss in intensity is related to reduction of the crystalline WO_3 NPs during metathesis. The corresponding simultaneous MS signals show that propylene metathesis is taking place with a ratio of only $C_2^=/C_4^=$ ∼ 0.1. The almost 1 order of magnitude decrease in formation of ethylene must be related to the significant amount of crystalline WO_3 NPs in the support 8% WO_x/SiO_2 catalyst (∼25%), since it is the only difference between the type

DOI: 10.1021/acscatal.6b00389
ACS Catal. 2016, 6, 3061−3071

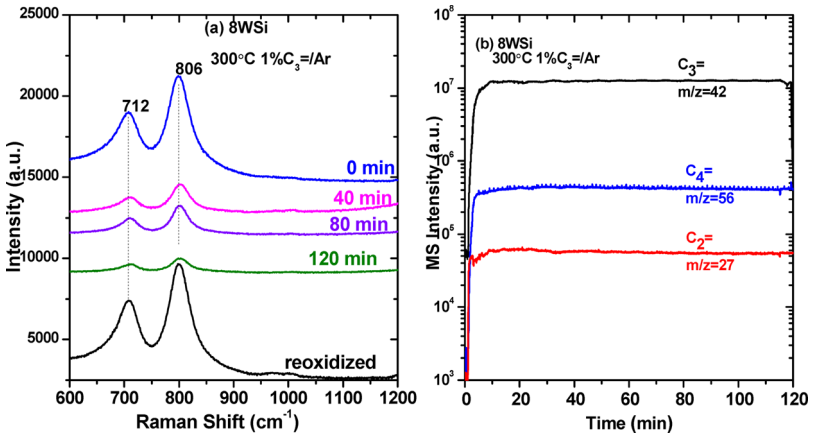

Figure 7. (a) *Operando* Raman spectra (442 nm) of the supported 8%WO_x/SiO_2 catalyst at 300 °C and (b) simultaneous MS spectra for the main products. The catalyst was reoxidized in 10% O_2/Ar at 500 °C for 30 min after the reaction (Raman spectra normalized against SiO_2 band at 495 cm^{-1} because of strong WO_3 band at 806 cm^{-1}). Propylene conversion was ∼9%.

of tungsten oxide sites in the supported 8% and 4% WO_x/SiO_2 catalysts. The formation of some polyaromatic coke on both catalysts is reflected by Raman bands at 1350 and 1600 cm^{-1} (SI Figure S6).

3.4. Activation of Supported WO_x/SiO_2 Catalysts at Constant Temperature (500 °C). The supported 8% WO_x/SiO_2 catalyst was activated by exposure to flowing $C_3^=$/Ar at 500 °C, and the results for the first 60 min are presented in Figure 8. The initial product is a spike of O_2 most probably

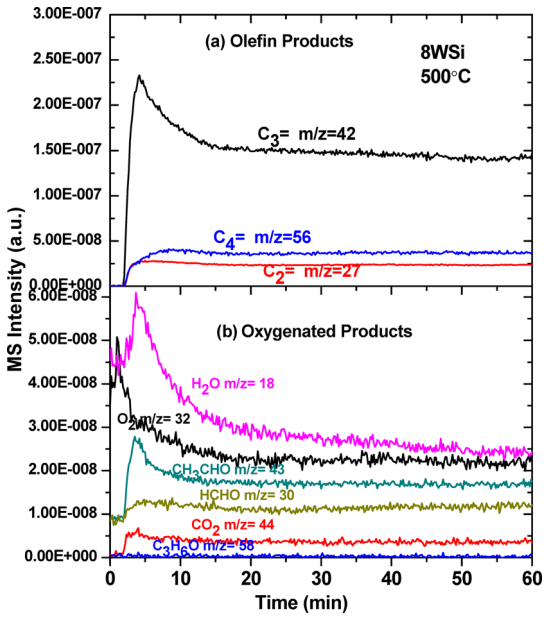

Figure 8. Activation of supported 8% WO_x/SiO_2 catalyst by flowing 1% $C_3^=$/Ar at 500 °C: (a) olefin products and (b) oxygenated products. Propylene conversion was ∼18%.

from displacement of a small amount of residual oxygen from the reactor by the flowing $C_3^=$/Ar. Immediately afterward, the metathesis of propylene to ethylene and butene reaction began, and oxygenated products (CH_3CHO, HCHO, H_2O and CO_2) also appear. Note that the oxygenated product acetone, CH_3COCH_3, was not detected.

3.5. Activation of Supported WO_x/SiO_2 Catalysts during TPSR Spectroscopy. The production of $C_4^=$ during activation of supported WO_x/SiO_2 in flowing $C_3^=$ in the temperature-programmed mode is presented in Figure 9 as a

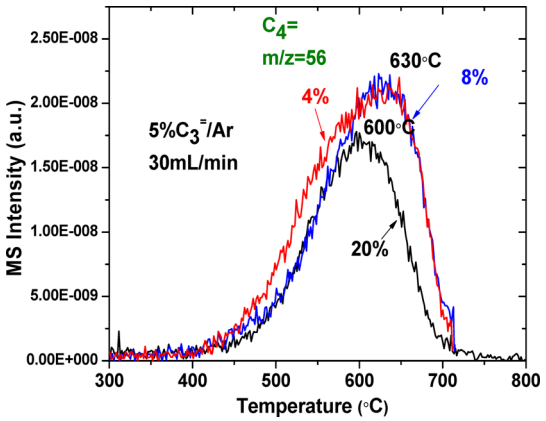

Figure 9. Production of $C_4^=$ during TPSR in flowing 5% $C_3^=$/Ar as a function of WO_x loadings. Other reaction products are shown in Figure S7.

function of WO_x loadings. The $C_4^=$-TPSR spectra for the supported 4% and 8% WO_x/SiO_2 catalysts are very similar (same Tp value), with the 4% WO_x/SiO_2 catalyst being slightly more active at the lower temperatures. The lack of increased production of $C_4^=$ in going from the 4% WO_x/SiO_2 to the 8% WO_x/SiO_2 catalyst reveals that the crystalline WO_3 NPs in the latter do not play a significant role in olefin metathesis and may actually diminish $C_4^=$ formation. This is further confirmed for the production of $C_4^=$ during TPSR with the 20% WO_x/SiO_2 catalyst, which consists of ∼65% WO_3 NPs, that yields even less formation of $C_4^=$. The leading edges for $C_4^=$ formation are almost the same for the 8% and 20% WO_x/SiO_2 catalysts.

The simultaneous evolution of H_2O and CO_2 during $C_3^=$ activation in the TPSR mode is presented in Figure 10. Formation of these oxidation products confirms the removal of oxygen atoms from the supported tungsten oxide phases on silica. The characteristics of H_2O evolution is dependent on the tungsten oxide loading. The supported 4% WO_x/SiO_2 catalyst, only containing the isolated surface WO_x sites, evolves H_2O in one major peak with Tp = 630 °C. The higher loading catalysts, containing both isolated WO_x sites and WO_3 NPs, exhibit two H_2O peaks at ∼485 and ∼630 °C. The production of H_2O at

DOI: 10.1021/acscatal.6b00389
ACS Catal. 2016, 6, 3061−3071

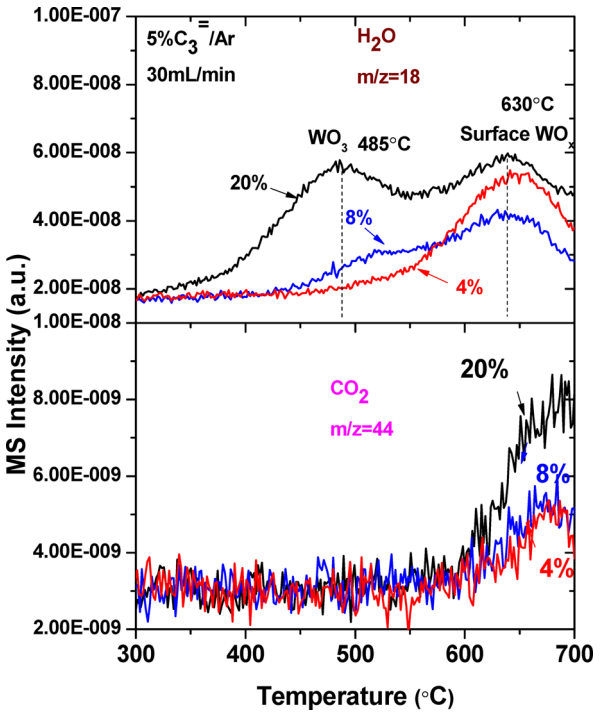

Figure 10. Production of H_2O and CO_2 in flowing 5% $C_3^=$/Ar as a function of WO_x loadings. The simultaneous conversion of $C_3^=$ and formation of $C_2^=$ are shown in Figure S7.

~630 °C is related to isolated surface WO_x sites on silica since this peak is observed for the 4% WO_x/SiO_2 catalyst that only contains isolated sites. The second H_2O peak at ~485 °C, however, is associated with the WO_3 NPs, and the intensity of this peak tracks their concentration in the catalysts. Integration of the H_2O-TPSR peaks indicates that the ~485 °C peak accounts for ~40% and ~60% of the total H_2O produced for the 8% and 20% WO_x/SiO_2 catalysts. These values reasonably track the amounts of crystalline WO_3 in these catalysts estimated above from XANES analysis. The evolution of CO_2 initiates at ~600 °C and peaks at ~680 °C. The formation of H_2O below 600 °C and formation of CO_2 above 600 °C suggests that some carbonaceous deposits are present on the catalyst during activation of the supported WO_x/SiO_2 catalysts by propylene below 600 °C

The influence of propylene in the gas phase on the supported 8% WO_x/SiO_2 catalyst preactivated with propylene at 500 °C for 45 min followed by additional exposure to propylene at 100 °C for 45 min is presented in Figure 11. When the TPSR is performed in flowing $C_3^=$-free Ar, no butene is formed. Performing TPSR in flowing $C_3^=$/Ar after the catalyst activation treatment produces butene at both ~220 and ~600 °C. The $C_4^=$ peak at ~600 °C is also observed during TPSR with an unactivated catalyst (see Figure 9), which suggests that the new low temperature $C_4^=$ peak is related to a new activated surface WO_x site. The $C_3^=$-TPSR findings also suggest that surface reaction intermediates are not stabilized on activated WO_x/SiO_2 catalysts, and the metathesis reaction requires the presence of propylene in the gas phase in order to proceed.

3.6. Steady-State Olefin Metathesis Reaction Studies.

The reaction rates (propylene molecules converted per g-cat per hour) and selectivity for propylene metathesis by the supported WO_x/SiO_2 catalysts as a function of tungsten oxide loading are presented in Figures 12 and 13, respectively. The

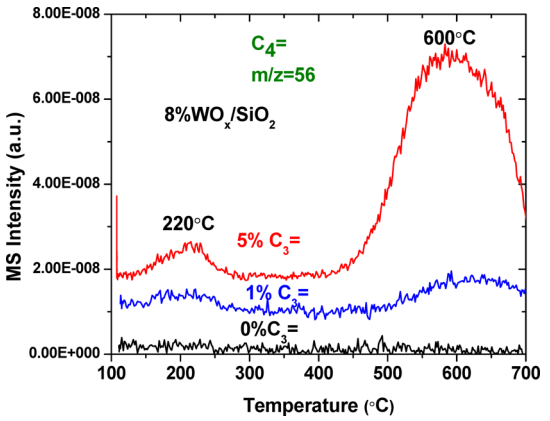

Figure 11. Production of $C_4^=$ during $C_3^=$-TPSR with 8% WO_x/SiO_2 catalyst in flowing $C_3^=$/Ar as a function of propylene concentration after a 500 °C $C_3^=$/Ar treatment for 45 min and $C_3^=$ adsorption at 100 °C before starting the $C_3^=$-TPSR. Other reaction products are shown in Figure S8.

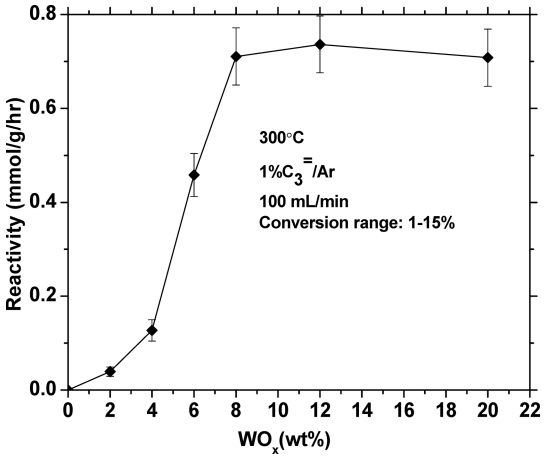

Figure 12. Propylene metathesis activity as a function of WO_x loadings for the supported WO_x/SiO_2 catalysts.

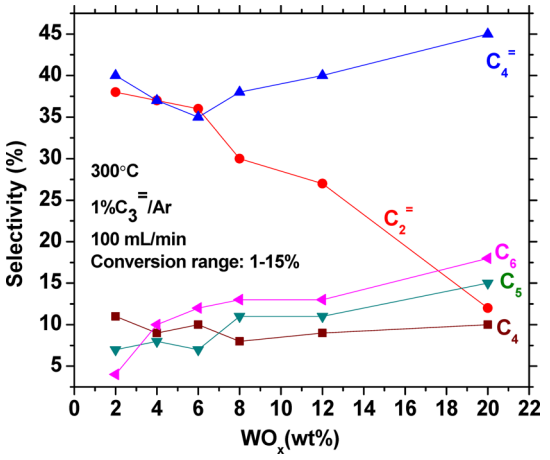

Figure 13. Propylene metathesis selectivity as a function of WO_x loadings for the supported WO_x/SiO_2 catalysts.

propylene metathesis reaction rate increases with tungsten oxide loading up to 8% WO_3/SiO_2 and then levels off for higher tungsten oxide loadings. Below 8% WO_3/SiO_2, only surface WO_x sites are present on the silica support and demonstrate

DOI: 10.1021/acscatal.6b00389
ACS Catal. 2016, 6, 3061−3071

that the reaction rate is proportional to the surface WO_x sites concentration (the catalytic active sites). Above 8% WO_3/SiO_2, the propylene metathesis reaction rate is relatively constant, reflecting the lack of influence of the WO_3 NPs upon reaction rate (not the catalytic active sites). The propylene metathesis $C_2^=/C_4^=$ selectivity is sensitive to the nature of the tungsten oxide sites present in the catalyst. Below 8% WO_x/SiO_2, where only surface WO_x sites are present, the ratio of $C_2^=/C_4^= \sim 1$, and ~20% C_4-C_6 alkane byproducts are also formed from the weak Lewis acids associated with the surface WO_x sites on SiO_2.[39] The selectivity to C_4 and C_5 is relatively constant, and the selectivity to C_6 increases with tungsten oxide loading from 2 to 6% WO_x/SiO_2. For 8% WO_x/SiO_2 and higher loadings, where crystalline WO_3 NPs are present in addition to the surface WO_x sites, the selectivity to $C_2^=$ dramatically decreases while the selectivity of $C_4^=$ modestly increases with tungsten oxide loading. The selectivity toward alkanes also further increases ($C_6 > C_5 > C_4$) with tungsten oxide loading with increasing amount of crystalline WO_3 NPs. These selectivity changes are thought to arise from the surface Brønsted acid sites associated with the crystalline WO_3 NPs.[40,41]

4. DISCUSSION

4.1. Molecular Structures of the Dehydrated Supported WO_x Sites on SiO_2. Under dehydrated conditions, isolated surface WO_x sites and crystalline WO_3 NPs are present on the SiO_2 support with their relative concentrations varying with tungsten oxide loading. At the lower loadings (<8% WO_3/SiO_2), the isolated nature of the surface WO_x sites on silica is reflected by the high UV−vis E_g value (~4.2−4.3 eV), lack of detectable bridging W−O−W Raman bending modes (~200−300 cm^{-1}) and absence of W in the EXAFS second coordination sphere (~3 Å). The surface WO_x sites are present as dioxo $(O=)_2W(-O)_2$ and mono-oxo $O=W(-O)_4$ with the concentration of the former much higher at lower tungsten oxide loadings (determined from the intensity of its *in situ* XANES pre-edge peak by comparison with reference compounds). For 8% WO_x/SiO_2 and higher tungsten oxide loadings, crystalline WO_3 NPs are also present in addition to the surface WO_x sites and their content increases with tungsten oxide loading (~25% for 8% WO_x/SiO_2 and ~60% for 20% WO_3/SiO_2). The appearance of WO_3 NPs coincides with the blue shift vibration for the surface WO_x sites, which may be related to their anchoring at more strained silica hydroxyl sites,[42] and a decrease in the dioxo/mono-oxo ratio. The ratio of dioxo/mon-oxo appears to be comparable in flowing O_2/He and He. In summary, two distinct surface WO_x sites are present on SiO_2 below 8% WO_x/SiO_2 and are accompanied by crystalline WO_3 NPs for 8% WO_x/SiO_2 and higher tungsten oxide loadings.

The literature for olefin metathesis by supported WO_x/SiO_2 catalysts seems to be confused about the molecular structures of the surface WO_x sites.[14−19] These publications assign the structure of the dehydrated surface WO_x sites on silica as being dioxo $(O=)_2W(-O)_2$, but their characterization measurements were performed under ambient conditions where the catalysts are wet and the sites are actually present as hydrated $W_{6-12}O_x$ clusters.[20,21] The current study, as well as our earlier publications,[20−23] reveal that two distinct isolated surface WO_x sites are present on SiO_2 at elevated temperatures where olefin metathesis is typically conducted with supported WO_x/SiO_2 catalysts.

4.2. Activation of Surface WO_x Sites and WO_3 NPs during Metathesis. At lower tungsten oxide loadings, the surface WO_x sites are activated during propylene metathesis by a loss of oxygen as shown by the (*i*) selective decrease in the intensity of the Raman bands for the supported WO_x sites (see Figure 6), (*ii*) appearance of UV−vis d−d bands (see Figure 2), and (*iii*) formation of oxygenated reaction products (see Figure 8). The decrease in the intensity of the Raman bands is from both removal of oxo W═O and coordination of olefins to the surface WO_x sites that results in band broadening. The absence of detectable Raman bands from the surface WO_x sites after 120 min of reaction suggests that 100% of the surface WO_x sites have become activated after extended reaction times. It is not possible to determine the molecular structures of the activated surface WO_x sites during olefin metathesis from the presented data and, in general, is quite difficult to ascertain since multiple surface tungsten oxide structures can possess the same oxidation states (e.g., $W^{6+}O_x$, $W^{6+}{=}CH_2$, $W^{6+}{=}CHCH_3$, and $W^{6+}O_3$ NPs when present).

At higher tungsten oxide loadings, where crystalline WO_3 NPs are also present, the WO_3 NPs also undergo partial reduction during activation with propylene since there is a loss of oxygen at lower temperatures when WO_3 NPs are present, as shown by the formation of oxygenated reaction products (see Figures 8 and 10), and a selective decrease in the Raman intensity of the WO_3 NPs (see Figure 7). This is especially evident for evolution of H_2O-TPSR at ~485 °C that is only formed when WO_3 NPs are present (see Figure 8). This suggests that partially reduced WO_{3-x} NPs are also present during propylene metathesis for high loaded silica-supported tungsten oxide catalysts.

All the supported surface WO_x sites on SiO_2 become activated by exposure to propylene at elevated temperatures (see Figures 7 and 11). The $C_3^=$-TPSR experiments, however, reveal that there are two distinct activated surface WO_x sites after high temperature activation with propylene since the formation of $C_4^=$ occurs at both ~220 and ~600 °C. The activated surface WO_x sites associated with the ~220 °C reaction, however, are $\sim 10^{11}$ times more active than the surface WO_x sites responsible for the ~600 °C reaction (assuming first-order kinetics and application of Redhead equation[43]). This strongly suggests that the surface WO_x sites associated with the ~220 °C reaction are the catalytic active sites when propylene metathesis is conducted below 500 °C and represents ~5−10% of the total surface WO_x sites on the SiO_2 support depending on WO_x loadings and $C_3^=$ partial pressure.

Although the supported WO_3 NPs also become activated by propylene at elevated temperatures, the resulting WO_{3-x} sites are not active for propylene metathesis since their presence does not affect the activity (see Figure 12).

Andreini and Mol claimed that a high temperature pretreatment in He (inert) both decreases the break-in time and improves the catalytic activity by a factor of 1.5 when the He pretreatment was performed at ~550 °C, and the reaction was run at ~380 °C.[44] However, Luckner and Wills performed both the He pretreatment and reaction studies at the same temperature of ~423 °C and found that although the He treatment decreases the break-in time, the catalytic activity is about the same over a longer period of 650 min (~11 h).[45] This discrepancy could be attributed to the different activation temperatures in both studies, and such pretreatment effects on number of catalytic active sites will be discussed in a subsequent communication.

DOI: 10.1021/acscatal.6b00389
ACS Catal. 2016, 6, 3061−3071

4.3. Surface Reaction Intermediates. Direct information about the nature of the surface reaction intermediates is not available from the characterization measurements performed in this study. The high reaction temperature required for propylene metathesis by supported WO_x/SiO_2 catalysts results in a very low concentration of surface reaction intermediates that is difficult to detect (*in situ* IR could not observe any reaction intermediates, which was not shown for brevity). This is also indicated by the need to have propylene in the gas phase in order for the metathesis reaction to proceed (see Figure 11).

Olefin metathesis for *trans*-2-butene and ethylene by crystalline WO_3 slabs was examined with DFT calculations by Cheng and Lo.[46,47] It was concluded that *trans*-2-butene more readily forms $W{=}CHCH_3$ intermediates than ethylene formation of $W{=}CH_2$ intermediates. Consequently, the $W{=}CHCH_3$ intermediates should propagate the metathesis reaction faster than the $W{=}CH_2$ intermediates and the [2 + 2] cycloaddition of *trans*-2-butene to form the oxametallacycle ring is the rate-determining step.[46] The use of crystalline WO_3 slabs in this DFT investigation is problematic since the experimental studies have demonstrated that crystalline WO_3 is not able to perform olefin metathesis and that the metathesis reaction occurs on the isolated surface WO_x sites.[6,48] DFT calculations with isolated surface WO_x sites would be more relevant to olefin metathesis by supported WO_x/SiO_2 catalysts and are expected to be reported in the near future.

4.4. Structure−Activity/Selectivity Relationships. The activity of the supported WO_x/SiO_2 catalysts for propylene metathesis is directly related to the concentration of surface WO_x sites as shown by the direct relationship between the increasing reaction rate with increasing amount of surface WO_x sites (see Figures 9 and 12). This structure−activity relationship implicates the surface WO_x sites as the catalytic active sites for propylene metathesis by supported WO_x/SiO_2 catalysts. As indicated above, the nature of the activated surface WO_x sites during propylene metathesis is presently not known. The Lewis acid character[39] of the surface WO_x sites on SiO_2 is responsible for the formation of some byproduct C_4−C_6 alkanes, and the formation of butane is the most sensitive to the concentration of surface WO_x sites.

It is difficult to determine the relative contributions of the isolated surface dioxo $(O{=})_2W(\text{-}O)_2$ and mono-oxo $O{=}W(\text{-}O)_4$ sites to propylene metathesis since both sites are always present in the same ratio for the supported <8% WO_x/SiO_2 catalysts and become activated in the olefin environment. It may be argued that the initial surface dioxo $(O{=})_2W(\text{-}O)_2$ site plays a more important role in olefin metathesis because of its much greater concentration in the initial catalyst since it represents ∼92% of the total surface WO_x sites. DFT calculations may be able to provide more insights about the reactivity of the two distinct surface WO_x sites. From DFT calculations of olefin metathesis by supported MoO_x/SiO_2 catalysts, which is the system most similar to supported WO_x/SiO_2, Handzlik concluded that coordinated dioxo pseudo-MoO_4 sites attached to two adjacent silanol groups are the catalytic active sites.[49] Furthermore, the five-coordinated mono-oxo surface MoO_5 site is not active for olefin metathesis because of the high activation barrier involved in both formation of cyclobutane intermediates and cyclo-reversal steps.[50]

The supported crystalline WO_3 NPs are not active for propylene metathesis as reflected in the lack of increase in reaction rate with increasing amount of crystalline WO_3 NPs (Figure 12). The supported crystalline WO_3 NPs adversely impact the olefin metathesis product selectivity (Figure 13), and their easier activation does not contribute to higher olefin metathesis activity (Figures 6 and 12). The Brønsted acid sites[39−41] present on the crystalline WO_3 NPs dimerize $C_2^=$ to $C_4^=$ as well as form additional C_4−C_6 alkanes.

The acidic characteristics of the surface WO_x sites and WO_3 NPs on SiO_2 account for the promotion of commercial supported WO_x/SiO_2 propylene metathesis catalysts with basic Na or K to neutralize the catalyst acid sites and minimize undesired dimerization of $C_2^=$ to $C_4^=$ as well as form the undesired C_4−C_6 alkane products.[48]

There are conflicting reports in the literature about the molecular structure−metathesis activity relationships for the supported WO_x/SiO_2 catalyst system. An early study by Thomas et al. claimed from Raman spectra collected under ambient conditions, XPS in a vacuum, and H_2-TPR studies that a high degree of dispersion and an easier reducibility are requirements for activity of both supported WO_x/SiO_2 and MoO_x/SiO_2 catalysts.[6] A more recent study by Hua et al. with supported WO_x/MTS-9 (titanium-silica sieve) concluded that WO_4 and WO_6 coordinated polytungstates are the catalytic active sites for metathesis rather than WO_3 NPs.[16] These reactivity findings are in agreement with the present study that the surface WO_x sites are the catalytic active sites for olefin metathesis and that WO_3 NPs do not contribute to olefin metathesis activity. The characterization measurements of the catalysts in the earlier studies, however, were performed under ambient conditions where the catalysts are hydrated and the WO_x structures are not relevant to olefin metathesis reaction conditions. The present study demonstrates that the surface WO_x are present as isolated dioxo $(O{=})_2WO_4$ and mono-oxo $O{=}WO_4$ sites prior to olefin metathesis and become partially reduced during olefin metathesis.

5. CONCLUSIONS

The supported WO_x/SiO_2 catalysts consist of isolated surface WO_x sites on silica (dioxo $(O{=})_2W(\text{-}O)_2$ and mono-oxo $O{=}WO_4$) and crystalline WO_3 NPs. Although both surface WO_x sites are activated by propylene by removal of oxygen, the dominant surface $(O{=})_2W(\text{-}O)_2$ is most likely the catalytic active precursor site. Activation produces a highly active catalytic site that can perform metathesis at modest temperatures (∼150−250 °C) and represents about ∼5−10% of the total surface WO_x sites. The concentration of surface reaction intermediates is very low because of the required elevated metathesis temperatures, and consequently, the reaction only proceeds in the presence of gas phase propylene. The crystalline WO_3 NPs become partially reduced to WO_{3-x} during propylene metathesis but are not able to perform the metathesis reaction. The Lewis and Brønsted acid character of the surface WO_x sites and WO_3 NPs, respectively, is responsible for the byproducts formed by $C_2^=$ dimerization to $C_4^=$ and oligomerization to C_4−C_6 alkanes. The present study represents the *first time* that molecular level structure−activity/selectivity relationships have been established for propylene metathesis by conventionally impregnated supported WO_x/SiO_2 catalysts.

■ ASSOCIATED CONTENT

Supporting Information

The Supporting Information is available free of charge on the ACS Publications website at DOI: 10.1021/acscatal.6b00389.

DOI: 10.1021/acscatal.6b00389
ACS Catal. 2016, 6, 3061−3071

Additional Raman, XANES/EXAFS, and TPSR figures (Figures S1−S8) (PDF)

AUTHOR INFORMATION

Corresponding Author

*E-mail: iew0@lehigh.edu.

Notes

The authors declare no competing financial interest.

ACKNOWLEDGMENTS

S.L. and I.E.W. gratefully acknowledge the financial support by the NSF Grant CHE 1301262. A.I.F. and Y.L. gratefully acknowledge funding of their work by the U.S. DOE Grant No. DE-FG02-03ER15476. We acknowledge the facilities support provided at the National Synchrotron Light Source at the Brookhaven National Laboratory (U.S. Department of Energy, Office of Basic Energy Sciences, Contract No. DE-SC0012704) and the Synchrotron Catalysis Consortium (U.S. Department of Energy, Office of Basic Energy Sciences, Grant No. DE-SC0012335).

REFERENCES

(1) Mol, J. C. *J. Mol. Catal. A: Chem.* **2004**, *213*, 39−45.
(2) Mol, J. C. *Catal. Today* **1999**, *51*, 289−299.
(3) van Schalkwyk, C.; Spamer, A.; Moodley, D. J.; Dube, T.; Reynhardt, J.; Botha, J. M.; Vosloo, H. C. M. *Appl. Catal., A* **2003**, *255*, 143−152.
(4) Spamer, A.; Dube, T. I.; Moodley, D. J.; van Schalkwyk, C.; Botha, J. M. *Appl. Catal., A* **2003**, *255*, 133−142.
(5) van Roosmalen, A. J.; Mol, J. C. *J. Catal.* **1982**, *78*, 17−23.
(6) Thomas, R.; Moulijn, J. A.; De Beer, V. H. J.; Medema, J. *J. Mol. Catal.* **1980**, *8*, 161−174.
(7) van Roosmalen, A. J.; Koster, D.; Mol, J. C. *J. Phys. Chem.* **1980**, *84*, 3075−3079.
(8) Verpoort, F.; Fiermans, L.; Bossuyt, A. R.; Verdonck, L. *J. Mol. Catal.* **1994**, *90*, 43−52.
(9) Verpoort, F.; Bossuyt, A.; Verdonck, L. *Chem. Commun.* **1996**, *3*, 417−418.
(10) Verpoort, F.; Bossuyt, A. R.; Verdonck, L. *J. Electron Spectrosc. Relat. Phenom.* **1996**, *82*, 151−163.
(11) Basrur, A. G.; Patwardhan, S. R.; Vyas, S. N. *J. Catal.* **1991**, *127*, 86−95.
(12) Martín, C.; Malet, P.; Solana, G.; Rives, V. *J. Phys. Chem. B* **1998**, *102*, 2759−2768.
(13) Davazoglou, D.; Moutsakis, A.; Valamontes, V.; Psycharis, V.; Tsamakis, D. *J. Electrochem. Soc.* **1997**, *144*, 595−599.
(14) Wang, Y.; Chen, Q.; Yang, W.; Xie, Z.; Xu, W.; Huang, D. *Appl. Catal., A* **2003**, *250*, 25−37.
(15) Hua, D.; Chen, S.; Yuan, G.; Wang, Y.; Zhang, L. *Transition Met. Chem.* **2011**, *36*, 245−248.
(16) Hua, D.; Chen, S.; Yuan, G.; Wang, Y.; Zhao, Q.; Wang, X.; Fu, B. *Microporous Mesoporous Mater.* **2011**, *143*, 320−325.
(17) Chaemchuen, S.; Phatanasri, S.; Verpoort, F.; Sae-ma, N.; Suriye, K. *Kinet. Catal.* **2012**, *53*, 247−252.
(18) Liu, N.; Ding, S.; Cui, Y.; Xue, N.; Peng, L.; Guo, X.; Ding, W. *Chem. Eng. Res. Des.* **2013**, *91*, 573−580.
(19) Huang, S.; Liu, S.; Zhu, Q.; Zhu, X.; Xin, W.; Liu, H.; Feng, Z.; Li, C.; Xie, S.; Wang, Q.; Xu, L. *Appl. Catal., A* **2007**, *323*, 94−103.
(20) Ross-Medgaarden, E. I.; Wachs, I. E. *J. Phys. Chem. C* **2007**, *111*, 15089−15099.
(21) Ostromecki, M. M.; Burcham, L. J.; Wachs, I. E.; Ramani, N.; Ekerdt, J. G. *J. Mol. Catal. A: Chem.* **1998**, *132*, 43−57.
(22) Lee, E. L.; Wachs, I. E. *J. Phys. Chem. C* **2007**, *111*, 14410−14425.
(23) Kim, D. S.; Ostromecki, M.; Wachs, I. E. *J. Mol. Catal. A: Chem.* **1996**, *106*, 93−102.
(24) Hamieh, A.; Chen, Y.; Abdel-Azeim, S.; Abou-hamad, E.; Goh, S.; Samantaray, M.; Dey, R.; Cavallo, L.; Basset, J. M. *ACS Catal.* **2015**, *4*, 2164−2171.
(25) Mougel, V.; Pucino, M.; Coperet, C. *Organometallics* **2015**, *34*, 551−554.
(26) Conley, M. P.; Mougel, V.; Peryshkov, D. V.; Forrest, W. P., Jr.; Gajan, D.; Lesage, A.; Emsley, L.; Coperet, C.; Schrock, R. R. *J. Am. Chem. Soc.* **2013**, *135*, 19068−19070.
(27) Bouhoute, Y.; Garron, A.; Grekov, G.; Szeto, K. C.; De Mallmann, A. D.; Del Rosal, I. D.; Maron, L.; Girard, G.; Gauvin, R. M.; Delevoye, L.; Taoufik, M.; Merle, N. *ACS Catal.* **2014**, *4*, 4232−4241.
(28) Mazoyer, E.; Merle, N.; Mallmann, A. D.; Basset, J.; Berrier, E.; Delevoye, L.; Paul, J.; Nicholas, C. P.; Gauvin, R. M.; Taoufik, M. *Chem. Commun.* **2010**, *46*, 8944−8946.
(29) Bouhoute, Y.; Grekov, D.; Szeto, K. C.; Merle, N.; De Mallmann, A. D.; Lefebvre, F.; Raffa, G.; Del Rosal, I. D.; Maron, L.; Gauvin, R. M.; Delevoye, L.; Taoufik, M. *ACS Catal.* **2016**, *6*, 1−18.
(30) Tian, H.; Roberts, C. A.; Wachs, I. E. *J. Phys. Chem. C* **2010**, *114*, 14110−14120.
(31) Stobie, K. M.; Bell, Z. R.; Munhoven, T. W.; Maher, J. P.; McCleverty, J. A.; Ward, M. D.; McInnes, R. J. L.; Totti, F.; Gatteschi. *Dalton Trans.* **2003**, 36−45.
(32) Seo, J. Ph.D. Dissertation, Brown University, 2013.
(33) Grunert, W.; Morke, W.; Feldhaus, R.; Anders, K. *J. Catal.* **1989**, *117*, 485−494.
(34) Yoshinaga, Y.; Kudo, M.; Hasegawa, S.; Okuhara, T. *Appl. Surf. Sci.* **1997**, *121/122*, 485−494.
(35) Horsley, J. A.; Wachs, I. E.; Brown, J. M.; Via, G. H.; Hardcastle, F. D. *J. Phys. Chem.* **1987**, *91*, 4014−4020.
(36) Balerna, A.; Bernieri, E.; Burattini, E.; Kuzmin, A.; Lusis, A.; Purans, J.; Cikmach, P. *Nucl. Instrum. Methods Phys. Res., Sect. A* **1991**, *308*, 240−242.
(37) Burcham, L. J.; Wachs, I. E. *Spectrochim. Acta, Part A* **1998**, *54*, 1355−1368.
(38) Chan, S. S.; Wachs, I. E.; Murrell, L. L. *J. Catal.* **1984**, *90*, 150−155.
(39) Macht, J.; Iglesia, E. *Phys. Chem. Chem. Phys.* **2008**, *10*, 5331−5343.
(40) Yang, X.; Dai, W.; Gao, R.; Fan, K. *J. Catal.* **2007**, *249*, 278−288.
(41) Ross-Medgaarden, E. I.; Knowles, W. V.; Kim, T.; Wong, M. S.; Zhou, W.; Kiely, C. J.; Wachs, I. E. *J. Catal.* **2008**, *256*, 108−125.
(42) Amakawa, K.; Sun, L.; Guo, C.; Havecker, M.; Kube, P.; Wachs, I. E.; Lwin, S.; Frenkel, A. I.; Patlolla, A.; Hermann, K.; Schlogl, R.; Trunschke, A. *Angew. Chem., Int. Ed.* **2013**, *52*, 13553−13557.
(43) Redhead, P. A. *Vacuum* **1962**, *12*, 203−211.
(44) Andreini, A.; Mol, J. C. *J. Colloid Interface Sci.* **1981**, *84*, 57−65.
(45) Luckner, R. C.; Wills, G. B. *J. Catal.* **1973**, *28*, 83−91.
(46) Cheng, Z.; Lo, C. *ACS Catal.* **2012**, *2*, 341−349.
(47) Cheng, Z.; Lo, C. *ACS Catal.* **2015**, *5*, 59−72.
(48) Spamer, A.; Dube, T. I.; Moodley, D. J.; van Schalkwyk, C.; Botha, J. M. *Appl. Catal., A* **2003**, *255*, 153−167.
(49) Handzlik, J. *J. Phys. Chem. B* **2005**, *109*, 20794−20804.
(50) Handzlik, J. *J. Phys. Chem. C* **2007**, *111*, 9337−9348.

DOI: 10.1021/acscatal.6b00389
ACS Catal. 2016, 6, 3061−3071